ACS APPLIED BIO MATERIALS

www.acsabm.org Article

Following the Aggregation of Human Prion Protein on Heparin Functionalized Gold Surface in Real Time

Tong Zhang, Yangang Pan, Sneha Kandapal, Xin Sun, and Bingqian Xu*

Cite This: ACS Appl. Bio Mater. 2022, 5, 5457−5464 Read Online

ACCESS | Metrics & More | Article Recommendations | Supporting Information

ABSTRACT: The aggregation of the prion protein (PrP) plays a key role in the development of prion diseases and is believed to be an autocatalytic process with a very high kinetic barrier. Intensive studies have focused on overcoming the kinetic barriers under extremely nonphysiological in vitro conditions by altering the pH of PrP solution on solid surfaces, such as gold, mica, and a lipid bilayer. Importantly, sulfated glycosaminoglycans (GAGs), including heparin, were found to be associated with PrP misfolding and aggregation, suggesting GAGs have catalytic roles in PrP aggregation processes. However, the exact role and details of GAGs in the PrP aggregation are not clear and need a thorough perusal. Here, we investigate the PrP aggregation process on a heparin functionalized gold surface by in situ, real-time monitoring of the atomic scale details of the whole aggregation process by single molecule atomic force microscopy (AFM), combining simultaneous topographic and recognition (TREC) imaging and single molecule force spectroscopy (SMFS). We observed the whole aggregation process for full-length human recombinant PrP (23−231) aggregation on the heparin modified gold surface, from the formation of oligomers, to the assembly of protofibrils and short fibers, and the formation of elongated mature fibers. Heparin is found to promote the PrP aggregation by facilitating the formation of oligomers during the early nucleation stage.

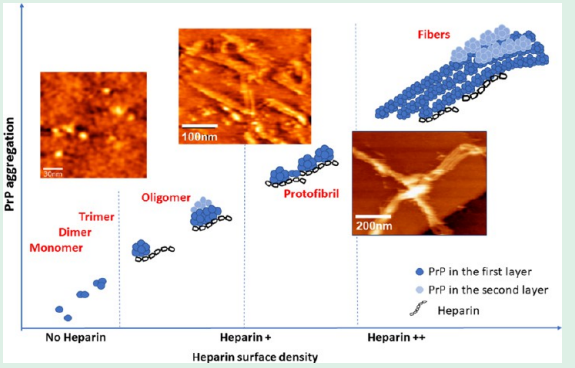

KEYWORDS: *prion protein (PrP) aggregation, aggregation morphology, heparin, nucleation stage, PrP−heparin interaction*

INTRODUCTION

"Prion" is a portmanteau word derived from "protein" and "infection", and can be considered a "proteinaceous infectious particle".[1] The pathogenic isoform of prion protein (PrP^{Sc}) is a noxious inducer of numerous fatal neurodegenerative diseases, such as Creutzfeldt−Jakob disease (CJD), Gerstmann−Straussler−Scheinker syndrome (GSS), fatal familial insomnia, and kuru.[2] The normal prion protein (PrP^{C}) is a signal transduction protein[3] ubiquitously expressed in various tissues, especially in neural progenitor cells as well as differentiated neural cells.[4] Under physiological conditions, PrP^{C} attaches to the outer leaflet of the plasma membrane via a glycosylphosphatidylinositol (GPI) anchor.[5] The widely accepted "protein only" hypothesis of prion aggregation/propagation postulates that these diseases are caused by the misfolding of a host-encoded glycoprotein, the prion protein (PrP^{C}) into a protease-insensitive isoform (PrP^{Sc}) that forms extended β-sheet-rich fibrillar PrP aggregations, as well as various on-pathway intermediates, such as long, ordered amyloid fibers, relatively small fibrils, and nonfibrillar β-sheet-rich oligomers, prior to the PrP fibrils.[6−14] However, in PrP aggregation, there is a very high kinetic barrier,[15−17] which was overcome by under extremely nonphysiological in vitro conditions, such as using surface and interface effects. For example, solid surfaces, such as gold, mica, graphite, Teflon, and lipid bilayer surfaces, have been shown to heavily influence the aggregation kinetics and the resulting aggregate morphology for a variety of amyloid-forming proteins.[16,18−22] In addition, the PrP aggregation is very complex process, and multiple factors such as exposure to an acidic environment[23] during endocytosis and extracellular matrix components[24,25] have been postulated to cause the pathological transition from PrP^{C} to PrP^{Sc} and promote PrP aggregation. Heparin, a highly sulfated heparan sulfate (HS),[26] is biosynthesized in mast cells and exists as membrane proteoglycans or is stored in cytoplasmic secretory granules,[27] and the negatively charged heparin molecules can bind to prion proteins with high affinity and thus affect the PrP aggregation process. Technically speaking, PrP aggregation processes have been intensively studied by circular dichroism (CD),[28] Thioflavin T fluorescence (ThT),[29] and nuclear magnetic resonance (NMR)[30]

Received: September 5, 2022
Accepted: October 6, 2022
Published: October 13, 2022

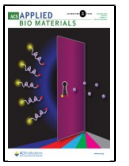

https://doi.org/10.1021/acsabm.2c00779
ACS Appl. Bio Mater. 2022, 5, 5457−5464

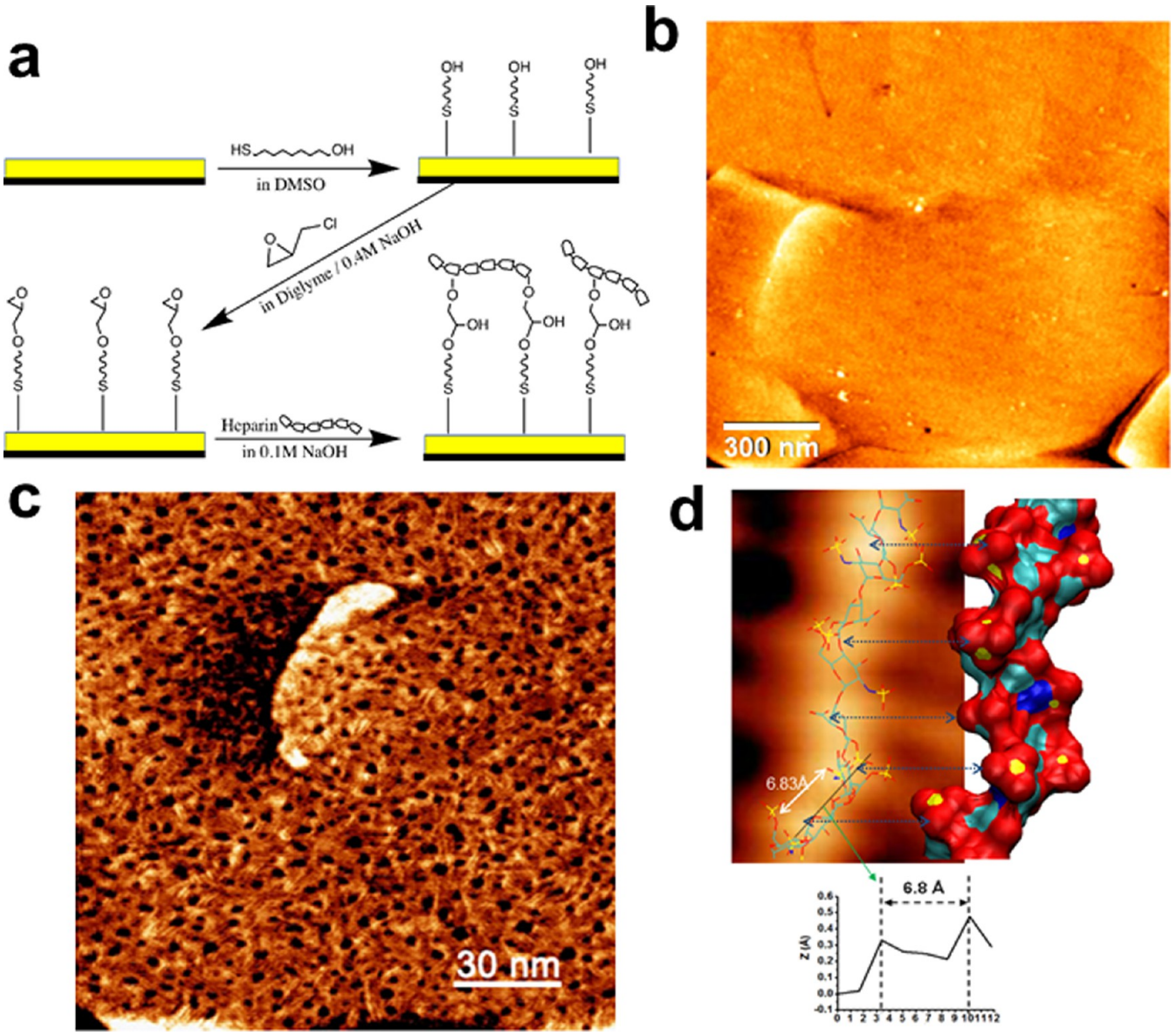

Figure 1. Immobilization of heparin on gold substrate. (a) The scheme for the heparin fixation on gold substrate. (b) Topographic image of gold surface modified with 100 μM heparin by TopMAC AFM. (c) STM images of heparin molecules on MUO monolayer. (d) The top is an enlarged area of the middle part of a heparin molecule from an STM topography image and heparin structure from an entire heparin molecule (PDB entry 3IRJ model 1). The labeled distance is the distance between two oxygen atoms on the sugar units O5S(SGN5)−O3S(SGN7). The bottom is the cross-section profile corresponding to the labeled distance in the top image.

which provided valuable insight into the conformational transition of the prion protein upon heparin binding. However, recent studies found that the toxicity of prion proteins is more closely related to the aggregation morphology, not the protein conformations.[2,31] For example, though fibrils may have properties similar to those of PrP^{Sc}, such as in the β-strand-rich structure and resistance to PK digestion, they are almost nonpathogenic.[32] On the contrary, PrP oligomers, which may experience a transient intermediate state,[33,34] exhibit more infectious capability than any other fibrillary structure.[35] Therefore, monitoring the PrP aggregation processes in real time may shed light into pathogenic transitions of PrP.

In this study, we monitored the PrP aggregation process on the heparin modified gold surface using in situ time-lapse atomic force microscopy (AFM). Remarkably, we found that heparin is not directly involved in the PrP assembly but only facilitates formation of oligomers nuclei during PrP aggregation, which is the rate-limiting step in the nucleation-dependent aggregation process. Because cell surface PrP−HS interaction could play a critical role in nucleating amyloid formation or altering aggregate morphology, this study will provide the single molecular level understanding of the roles of HS in PrP aggregation in a more physiologically relevant way.

EXPERIMENTAL SECTION

Heparin Functionalized Au(111) Surface. The gold substrate was prepared by thermally evaporating a gold layer on a freshly cleaved mica surface and then annealed under a hydrogen flame for 4 min to form a flat Au(111) structure. Heparin was immobilized on the 11-mercapto-1-undocanol (MUO) modified Au(111) surface through an epoxy group activated hydroxyl groups reaction (SI-2). High resolution scanning tunneling microscope (STM) imaging was performed in PBS buffer to visualize the atomic scale structure and

https://doi.org/10.1021/acsabm.2c00779
ACS Appl. Bio Mater. 2022, 5, 5457−5464

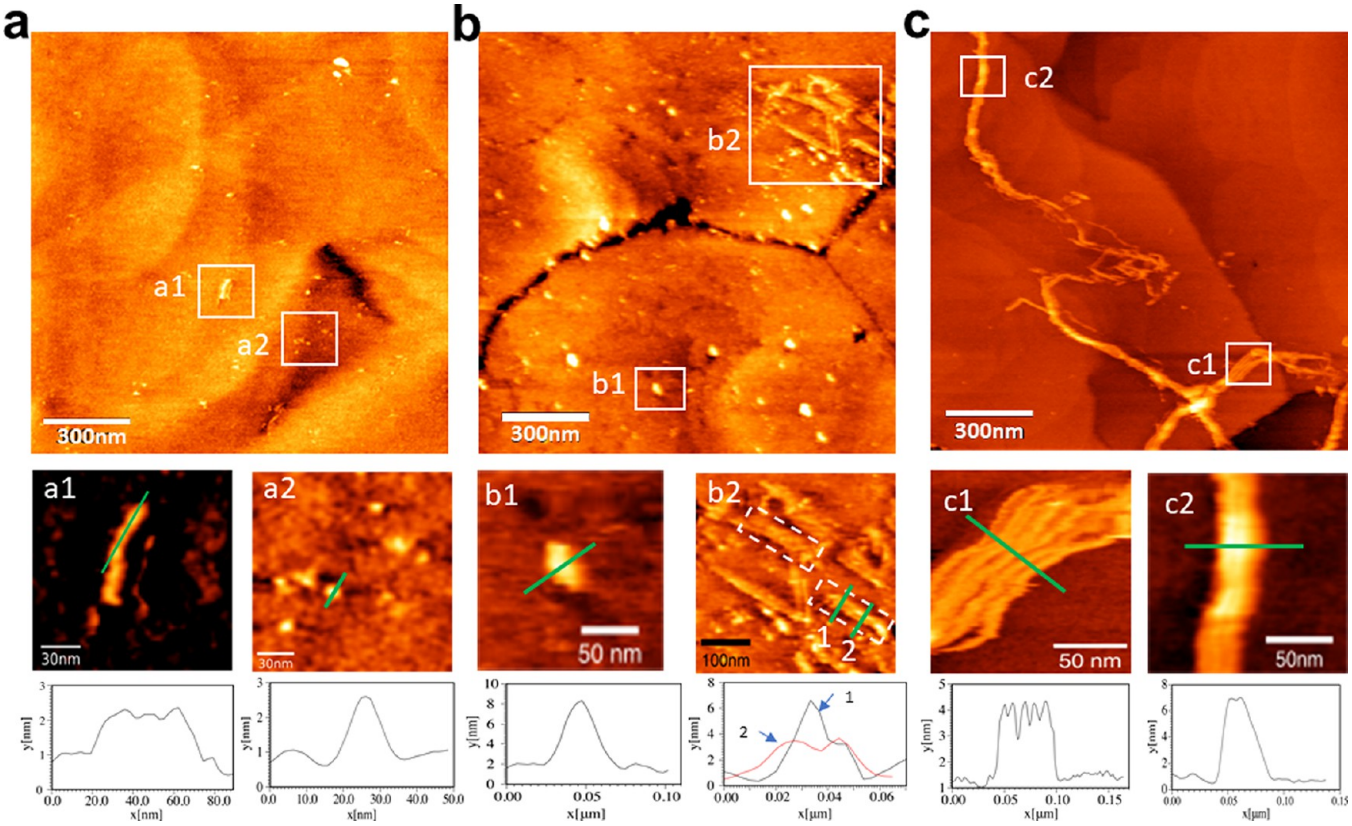

Figure 2. The PrP aggregation on different concentrations of the heparin modified surface. (a) The topographic image of PrP aggregation on MUO surface without heparin. (a1, a2) Zoom-in images of protofibrils and oligomers from the white squares in panel a. (b) The topographic image of PrP aggregation on the low concentration heparin modified surface. (b1, b2) Zoom-in images from the white squares in panel b. (c) The topographic image of PrP aggregation on the high concentration heparin modified surface. (c1, c2) Zoom-in images from the white squares in panel c. The cross-section profiles of the green lines are shown at the bottom of the corresponding images.

compared to the MD simulated structure (PDF entry 3IRJ model 1) (SI-4).

AFM Imaging and Measuring of PrP Aggregation. AFM experiments including imaging and force−distance curve measurements were carried out using an Agilent 5500 AFM system (Agilent, Chandler, AZ). Silicon cantilever tips with a spring constant of around 0.1 N/m were used for experiments. The AFM tip was magnetically coated and further coated with a second layer of gold (SI-3). A multipurpose closed loop scanner (N9524A, Keysight, Santa Rosa, CA, USA) with TopMAC nose cone cantilever modules was used to perform the topographic and recognition imaging and force spectroscopy in PicoTREC mode. For recognition imaging and the binding force measurements, the AFM tip was functionalized with antithrombin (AT) and PrP with heterobifunctional PEG linkers (HS-PEG-NHS and HS-PEG-COOH). The HS-end of the PEG linker bonds to the Au-coated tip via a strong Au−S bond, and PrP was linked on the AFM tip by the reaction between its amino group and *N*-hydroxysuccinimidyl ester while antithrombin molecules were linked on AFM tips through the reaction between the ε-ammonium group of lysine and −COOH on the linker (SI-3). From the recognition images with nanometer resolution, the binding sites were recognized, and the AFM was then switched to force spectroscopy mode, using the close-loop position feedback control.

Data Analysis. All of the imaging data were processed using a free scanning probe microscopy software WSxM 5.0. Force spectroscopy data were processed using our homemade LabView programs.

RESULTS AND DISCUSSION

Immobilization of Heparin on Gold Substrate. Heparin molecules were fixed on flat Au(111) surface through MUO and epichlorohydrin (Figure 1a). Though Au is a noble metal, it can form Au−S covalent bond[36] with the -SH group on the MUO. Heparin was then covalently connected to the epoxy groups at the MUO terminal by the hydroxyl groups of heparin sugar rings. (see SI-1 and SI-2 in the Supporting Information). AFM image (Figure 1b) shows a large area (1 μm^2) of the gold surface modified with 100 μM heparin. In order to determine the details of the immobilized heparin molecules, we measured the length and height of individual heparin molecules from 20 small area AFM images (200 nm^2) (see Figure SI-1). The height of heparin molecule is determined to be around 0.3 nm, agrees with our previous result of 0.19 ± 0.03 nm determined by AFM imaging[37] and the high resolution STM imaging (Figure 1d). Heparin is a flexible linear molecule that could randomly twist in the solution. However, the conformation of heparin after fixation were influenced by the number of linkages to the surface, as every hydroxyl group in the disaccharides of heparin may form covalent bond with the surface. A high molecular weight heparin possesses over 20 disaccharides may adopt stretched linear or partially twisted conformations with multiple fixation degrees, which is clearly shown by the STM image (Figure 1c). Therefore, there should be different lengths of the immobilized heparin. The average length of heparin was determined statistically using the length histogram to be 16.90 ± 6.04 nm, agrees well with the 17 nm length measured by the X-ray crystal structures (3IRJ, 24 disaccharides, Mw of 13.5 kDa).[38] Remarkably, the topography image in Figure 1d presented the atomic scale details of a part heparin chain from one single

https://doi.org/10.1021/acsabm.2c00779
ACS Appl. Bio Mater. 2022, 5, 5457−5464

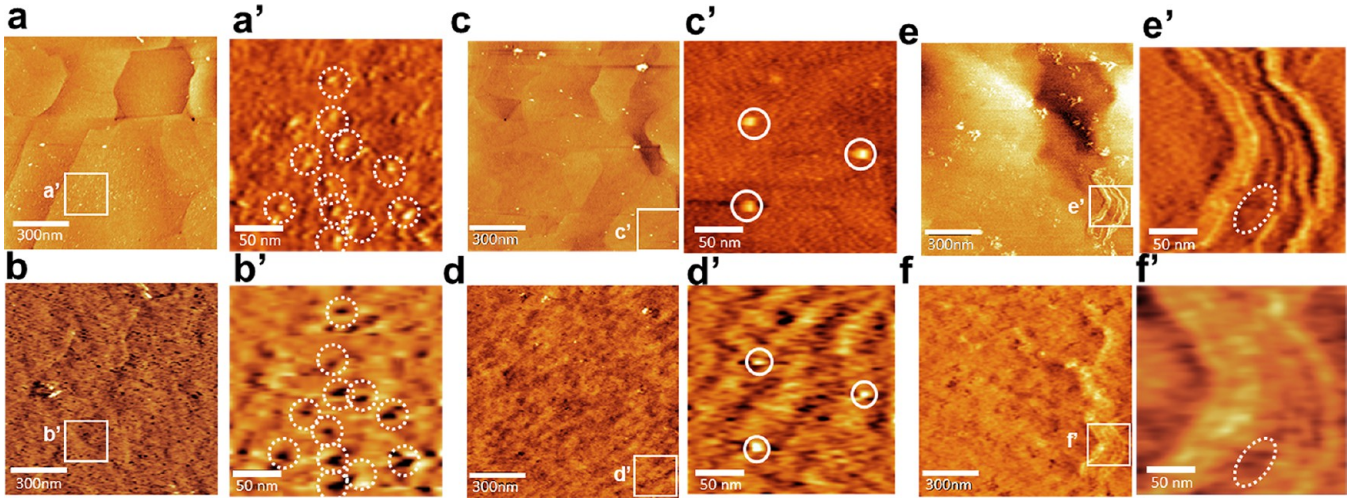

Figure 3. Time-lapse AFM images of PrP aggregation on the high concentration heparin modified surface. Top panel shows topographic images where panels a, c, and e are the topographic images (1 μm^2) of PrP on heparin modified surface obtained at 0, 5 h, and 7 h of PrP incubation, respectively. Panels b, d, and f are corresponding recognition images of panels a, c, and e. (a′, c′, e′ and b′, d′, f′) Zoomed-in small area (200 μm × 200 μm) topographic and recognition images.

heparin filament, including some discrete spherical cores flanked by short "sulfate arms". The spherical cores are sugar units of heparin according to the simulated structure. The distance between the "sulfate arms" in the STM image (black line) was around 6.8 Å, which agreed well with the simulated 6.83 Å distance from one oxygen atom in the O-sulfate group to another oxygen atom in the sulfamate group. More comparisons of the distances from the STM image and the simulated structure were given in Figure. S2, which showed excellent agreement. Therefore, the sulfate groups on the heparin filament were successfully distinguished on the STM images.

Influence of Heparin Concentration on PrP Aggregation. We first started with PrP aggregation on a MUO surface without heparin. Similar to the previous experimental result on the mica surface[20] in which the spontaneous PrP aggregation is a slow process, 5 h after adding 400 μL of 100 ng/mL PrP on the MUO surface without heparin, the small oligomers sporadically emerged on the MUO surface (Figure 2a) with a width of 18 nm and a height of 1.5 nm (Figure 2a2). Meanwhile, we also observe that the free oligomers on the surface could assemble and elongate into the short protofibrils (Figure 2a1). Because MUO could form a covalent bond with a gold atom through a thiol group, the hydrophilic hydroxyl groups thus are left to the aqueous environment, forming a similar physical environment to the mica surface.

However, in the presence of heparin, the aggregation morphologies were significantly different in a sense that the PrP molecules could aggregate into much larger oligomers or even assemble into mature fibrils. On the 8 μM heparin modified surface, the most prevalent morphology is the oval oligomers (Figure 2b) with 50 nm width and 6−7 nm height (Figure 2b1). In addition, the formation of short PrP fibrils was observed in the heparin modified surface, which was absent on the MUO surface. The fibers could be either a single strand or multiple laterally aligned strands (Figure 2b2, dashed white rectangle) at a height of 3.5 nm. Interestingly, PrP molecules could also further be deposited on top of the existing fibers, forming a second layer of fiber and doubling the height of the fibrils (Figure 2b2).

In contrast to the PrP aggregation morphology on the low heparin concentration modified surface, a high heparin concentration (100 μM) resulted in the formation of huge amyloid fibers several micrometers long with only a few oligomers in oval or spherical shapes distributed alongside the mature fibers (Figure 2c). Though the fibers on the high concentration heparin modified surface were much longer and condensed with more lateral strands than those on the low concentration heparin modified surface, they shared similar properties. For example, both of the fibers had the similar height of 3.5 nm with multiple parallel strands aligned side-by-side (Figure 2b2,c1). In addition, the PrP oligomers may exactly accumulate on the top of the first layer of fiber, forming a second layer of PrP fibrils (Figure 2b2,c2).

The Role of Heparin in the PrP Aggregation. In order to observe the role of heparin in the PrP aggregation, we imaged PrP aggregation on the high concentration (100 μM) heparin modified surface with the antithrombin (AT) functionalized tips by simultaneously recording the topography and PicoTRAC recognition images by analyzing the downward and upward parts of the oscillation, respectively.[39,40] Corresponding to the topographic images, the entities recognized are recorded as dark areas in the recognition image. AT, a well-known anticoagulant, is specific in recognizing the 3-*O*-sulfated pentasaccharides of heparin[39] and is thereby used for tracing the signal of heparin molecules on the surface. Figure 3 shows the 7 h in situ and real time AFM topographic (top panel) and recognition (bottom panel) images monitoring PrP aggregation. Our results clearly show that the PrP aggregation starts with a rate-limiting slow process of the formation of oligomers from the small monomer, dimer, and trimer in the first 5 h (Figure 3c), followed by a much faster process of the assembly of protofibrils, short fibers, and elongated mature fiber (Figure 3f), indicating that the slowly formed the oligomers can quickly assemble themselves into the advanced structures such as protofibrils or short fibrils. Meanwhile, the simultaneously recorded recognition images show the location and distribution of heparin molecules (shown as dark dots in the bottom panel of Figure 3). Generally, the recognition area as marked with the white

https://doi.org/10.1021/acsabm.2c00779
ACS Appl. Bio Mater. 2022, 5, 5457−5464

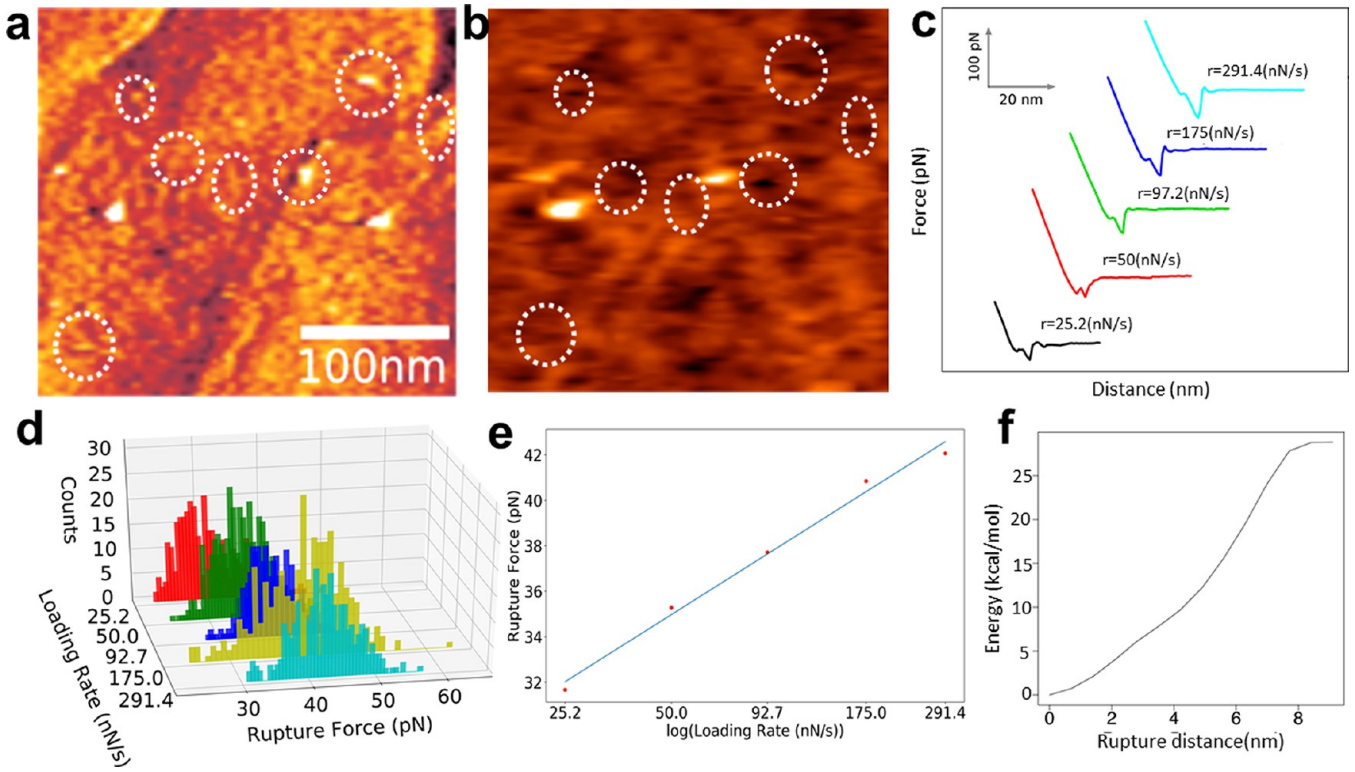

Figure 4. PrP−heparin interactions. (a, b) Topography (a) and recognition (b) images of heparin modified gold surface. (c) Representative retracting curves at 5 different loading rates. (d) Histogram distributions of rupture forces of the corresponding 5 different loading rates. (e) Linear fitting of rupture force and logarithmic loading rates. (f) The reconstructed free energy profile for PrP−heparin interaction.

dotted circles gradually decreased with time passing, suggesting that the PrP covers the surface of heparin and thus blocked the interaction between heparin and AT because AT does not bind to PrP. Specifically, prior to adding PrP, the heparin molecules on the gold surface (Figure 3a,a′) could be recognized by the AT functionalized AFM tip (dark dots in Figure 3b,b′). Five hours after PrP was added through a scanning liquid cell, PrP monomer, dimer, and trimer species are observed on the gold surface forming oligomers (Figure 3c). The highlighted bright dots in Figure 3c′ and the corresponding dots in d′ mark the PrP oligomer locations. It is clear that they are not recognized by the AT molecules hanging on the AFM tip, as they are also bright dots in d′, not the expected dark dots if they are recognized. The fact that AT molecules attached to the apex of the tips can only be recognized by heparin molecules but not PrP molecules explains the absence of dark recognition spots in the corresponding positions in the white solid circles (Figure 3c′,d′). After 7 h, finally, matured PrP fibers were formed where one fiber bundle may consist of multiple parallel protofibrils (Figure 3e,e′), with a height of about 3 nm. However, the fibers do not show any recognition signals on the corresponding recognition image (Figure 3f,f′), except the exposed heparin area between the fibers (highlighted with the dotted ovals). This demonstrated that heparin could facilitate the formation of fibril building blocks, oligomers, but not directly be involved in the larger protofibrils and giant fiber assembly process.

PrP−Heparin Interactions. SMFS is used to probe and characterize PrP−heparin interactions on the single molecular level to quantify the kinetics of the interaction between the PrP functionalized tip (see SI-3) and gold surface modified with 100 μM heparin. Figure 4a,b shows simultaneously obtained topography and recognition images of heparin molecules providing the binding sites (examples highlighted with white dotted circles). The advantage of such TREC-driven force spectroscopy is that a single functional molecule can be selected and targeted for force spectroscopy with high specificity. Figure 4c shows representative rupture forces under a different force loading rate (r) at 25.2, 50.0, 97.2, 175.0, and 291.4 nN/s. The constructed force histograms from over 300 curves for each loading rate results in the rupture force of 31.67 ± 4.90, 35.28 ± 4.13, 37.72 ± 3.61, 40.86 ± 6.09, and 42.07 ± 4.53 pN, respectively (Figure 4d). According to the Bell−Evans model,[41] the force (F) and logarithmic loading rate ($\ln(r)$) were fit linearly into the equation (eq 1):

$$F = \left(\frac{k_B T}{x_B}\right) \ln \frac{r x_B}{k_0 T k_B} \quad (1)$$

where x_B is energy barrier width, k_0 is the kinetic off-rate, k_B is the Boltzmann constant, and T is the absolute temperature. This resulted in $F = 4.311 \times \ln(r) + 18.109$ (Figure 4e). The equilibrium parameters x_B and k_0 were thus determined to be 0.83 nm and 0.0034 s^{-1}. Compared to the energy barrier width estimates of the interaction between heparin and FX06 or heparin and antithrombin which are 0.31 nm[37] and 0.46 nm,[42] respectively, the larger x_B between PrP and heparin may result from the protein conformational change during the pulling process. PrP has been demonstrated to extend 9 ± 1 nm from the native state to the unfolded state under a constant force of 11 pN[17] which is lower than the rupture force between PrP and heparin. Thus, the energy barrier width of 0.35−0.42 nm of the protein unfolding transition[43] may also partially contribute to x_B of the heparin and PrP interaction. As for

https://doi.org/10.1021/acsabm.2c00779
ACS Appl. Bio Mater. 2022, 5, 5457−5464

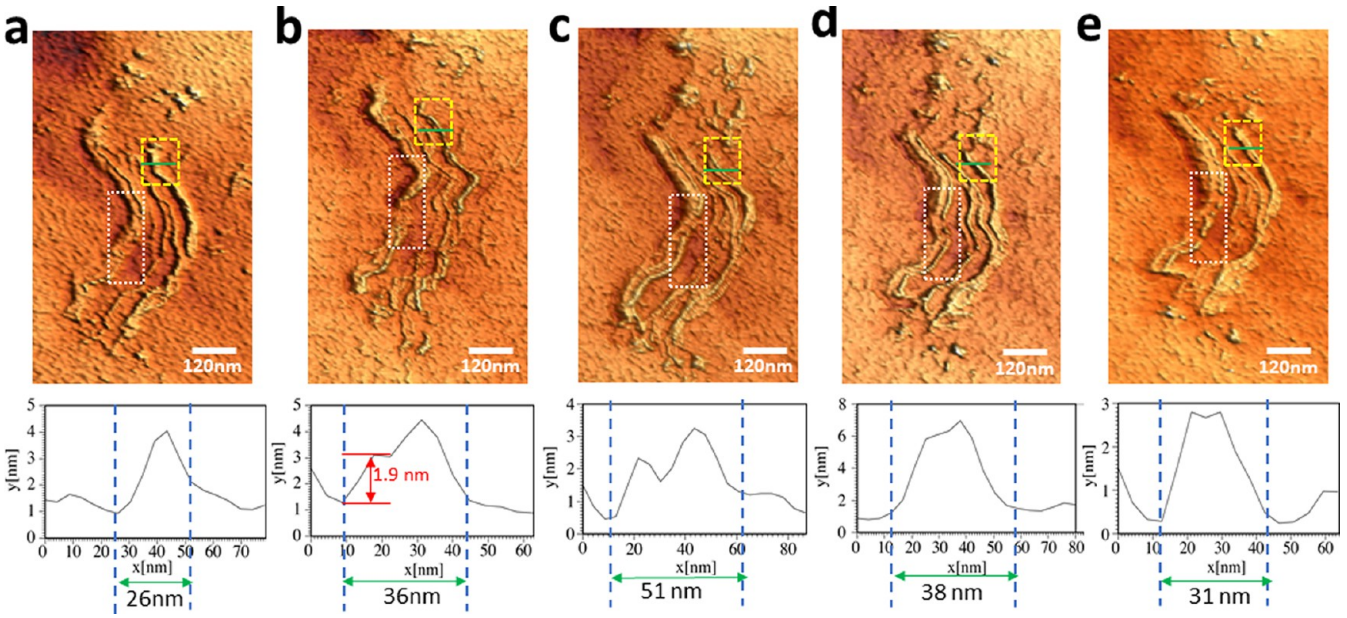

Figure 5. 3D images of PrP fibers acquired by in situ time-lapse AFM. (a) The image of short fibrils after adding PrP on the high concentration heparin fiber for 5 h. (b–e) Images acquired 7, 20, 40, 61 min after panel a. The cross-section profiles of the green lines are shown at the bottom of corresponding images.

the kinetic off-rate k_0, 0.0034 s^{-1} for the PrP–heparin interaction is less than the 0.04 s^{-1} for heparin and antithrombin,[44] suggesting that the PrP could dissociate from heparin more quickly than antithrombin. The difference in k_0 rate might be the underlying basis for the rapidly reversible binding of PrP oligomers to the heparin modified surface in the time-lapse imaging experiment.

Another important thermodynamic quantity we determined from force spectroscopy data is the Gibbs free energy associated with the binding between PrP and heparin. According to the elegant Jarzynski equality (eq 2):

$$\langle e^{-\beta W}\rangle N \equiv e^{-\beta \Delta G} \quad (2)$$

where $\beta = (1/kBT)$, kB is the Boltzmann constant, and T is the temperature. The left side of eq 2 represents an average over N realizations of the process. Theoretically, it has been shown that the equality is exact in the limit $N \rightarrow \infty$.[45] Through reconstructing the force trajectory by an exponentially weighted averaging of 349 force–distance curves (Figure S3), the Gibbs free energy profile was rebuilt (Figure 4f). The related change in Gibbs free energy (ΔG) for PrP–heparin interaction was calculated to be 28.53 kcal/mol. Interestingly, it is larger than the ~20 kcal/mol energy barrier biochemically determined to trap the native structure from a more thermodynamically stable, β-rich oligomeric state[46] and 64 ± 6 kJ/mol (~14 kcal/mol) energy barrier from the native state determined by single molecule optical trapping.[17] Considering that the rupture lengths under different loading rates are 6.04 ± 0.37, 6.40 ± 0.37, 5.76 ± 0.69, 6.04 ± 0.45, and 5.60 ± 0.33 nm, respectively, the PrP protein could be partially unfolded during the pulling processes,[45] and our measured ΔG may include both the Gibbs free energy of the interaction between heparin and PrP and the energy in the PrP conformational change, i.e., partial PrP unfolding. Further detailed investigations are needed from this perspective.

The Dynamic Process of PrP Fiber Formation. Now we have experimentally established that the oligomers are the basic units of protofibrils and fibers. Further, the detailed behavior of the oligomers during the fibril growing process is also revealed. The images in the white dashed rectangle in Figure 5 record the association and dissociation process of oligomer on the surface during the formation and growing of the PrP fiber. At the beginning of the monitoring, a few small oligomers were found to sporadically deposit on the surface from the original fibrils (Figure 5a). With more oligomers polymerized and attached to the existing oligomers (Figure 5b,c), an intact fiber gradually emerges (Figure 5d). However, certain oligomers that were part of the short fiber spontaneously dissociated from the advanced fibril structure, leaving a scattered fibril skeleton in place (Figure 5e). This result demonstrated that the elongation of PrP fibrils is also a dynamic process.

The time-series images in the dashed green rectangle represent the formation of lateral fibrils (Figure 5). Compared with the zero-time point (Figure 5a), two oligomers at the height of 1.9 nm are attached to the existing 26 nm wide single fiber strand after 7 min, and the width grows to 36 nm (cross-section profile in Figure 5b). As the R-squared value of the oligomer height is around 0.89 nm,[20] 1.9 nm represents two oligomers stacking vertically. At 20 min, more oligomers are accumulating to form a new parallel strand (Figure 5c) at a similar height of oligomers with the width further growing to 51 nm. Afterward, additional PrP molecules are inserted into the groove of the two fibrils and formed a second layer of PrP fibril, increasing the height of the fibrils to 5.4 nm with the width shrinking to 38 nm (Figure 5d). After another 21 min, the second layer PrP dissociates from the first layer (Figure 5e). As a result, two lateral fibrils get exposed at the height of 2.7 nm with the width of 31 nm. The height and width changes may be induced by the conformational change of PrP during intermolecular interactions of the oligomers or the attachment of additional PrP monomer, dimer, or trimer, whose heights are about 0.8–1.2 nm, in the fibril assembly. The above observation indicates that not only is the surface attachment of

https://doi.org/10.1021/acsabm.2c00779
ACS Appl. Bio Mater. 2022, 5, 5457–5464

oligomers a reversible process, but also the association between oligomers in the advanced morphology is a dynamic process as well. Contrary to the rapid turnover of PrP oligomers or short protofibrils on the heparin modified surface, the skeletons of fibril could stay on the surface for an extended period of time.

CONCLUSION

Through combining simultaneous topographic and recognition (TREC) imaging and single molecule force spectroscopy (SMFS), the atomic scale details of the whole PrP aggregation on heparin functionalized gold surface were monitored in situ and in real time. We find that the aggregation morphologies were significantly different in the presence of heparin in a sense that the PrP molecules could aggregate into much larger oligomers or even assemble into mature fibrils while only PrP oligomers form in the absence of heparin. The process of forming the PrP fiber is found to be a dynamic association and dissociation of oligomer as revealed by flowing detailed behavior of the oligomers during the fibril growing process with time-series images. Remarkably, we found that heparin is not directly involved in the PrP assembly but only facilitates formation of oligomers nuclei during PrP aggregation, which is the rate-limiting step in the nucleation-dependent aggregation process. Because the cell surface PrP−HS interaction could play a critical role in nucleating amyloid formation or altering aggregate morphology, this study will provide the single molecular level understanding of the roles of HS in PrP aggregation in a more physiologically relevant way.

ASSOCIATED CONTENT

Supporting Information

The Supporting Information is available free of charge at https://pubs.acs.org/doi/10.1021/acsabm.2c00779.

Details on chemicals and materials, immobilization of heparin on gold substrate, functionalization of AFM tips with antithrombin (AT) and PrP, AFM imaging and force−distance curve measurement, comparison of STM images and simulated heparin structure, and the process of calculating Gibbs free energy profile of PrP−heparin interaction (PDF)

AUTHOR INFORMATION

Corresponding Author

Bingqian Xu − *Single Molecule Study Laboratory, College of Engineering and Nanoscale Science and Engineering Center, University of Georgia, Athens, Georgia 30602, United States;* orcid.org/0000-0002-7873-3162; Email: nanoxu@uga.edu

Authors

Tong Zhang − *Single Molecule Study Laboratory, College of Engineering and Nanoscale Science and Engineering Center, University of Georgia, Athens, Georgia 30602, United States*

Yangang Pan − *Single Molecule Study Laboratory, College of Engineering and Nanoscale Science and Engineering Center, University of Georgia, Athens, Georgia 30602, United States;* Present Address: Department of Anesthesiology, Weill Cornell Medical College, New York, NY 10021, United States

Sneha Kandapal − *Single Molecule Study Laboratory, College of Engineering and Nanoscale Science and Engineering Center, University of Georgia, Athens, Georgia 30602, United States;* orcid.org/0000-0002-3572-1487

Xin Sun − *Single Molecule Study Laboratory, College of Engineering and Nanoscale Science and Engineering Center, University of Georgia, Athens, Georgia 30602, United States;* orcid.org/0000-0003-3153-8615

Complete contact information is available at: https://pubs.acs.org/10.1021/acsabm.2c00779

Author Contributions

The manuscript was written through contributions of all authors. All authors have given approval to the final version of the manuscript.

Notes

The authors declare no competing financial interest.

ACKNOWLEDGMENTS

This work was partially supported by US National Science Foundation (ECCS 1231967 and 2010875).

REFERENCES

(1) Prusiner, S. B. Novel proteinaceous infectious particles cause scrapie. *Science* **1982**, *216* (4542), 136−144.

(2) Aguzzi, A.; Calella, A. M. Prions: protein aggregation and infectious diseases. *Physiol. Rev.* **2009**, *89* (4), 1105−1152.

(3) Didonna, A. Prion protein and its role in signal transduction. *Cell. mol. biol. lett.* **2013**, *18* (2), 209.

(4) Mouillet-Richard, S.; Ermonval, M.; Chebassier, C.; Laplanche, J. L.; Lehmann, S.; Launay, J. M.; Kellermann, O. Signal transduction through prion protein. *Science* **2000**, *289* (5486), 1925−1928.

(5) Kazlauskaite, J.; Sanghera, N.; Sylvester, I.; Vénien-Bryan, C.; Pinheiro, T. J. T. Structural changes of the prion protein in lipid membranes leading to aggregation and fibrillization. *Biochemistry* **2003**, *42* (11), 3295−3304.

(6) Caughey, B.; Lansbury, P. T. Protofibrils, pores, fibrils, and neurodegeneration: Separating the responsible protein aggregates from the innocent bystanders. *Annu. Rev. Neurosci.* **2003**, *26*, 267−298.

(7) Fridmanis, J.; Toleikis, Z.; Sneideris, T.; Ziaunys, M.; Bobrovs, R.; Smirnovas, V.; Jaudzems, K. Aggregation Condition-Structure Relationship of Mouse Prion Protein Fibrils. *Int. J. Mol. Sci.* **2021**, *22* (17), 9635.

(8) Goldberg, M. S.; Lansbury, P. T. Is there a cause-and-effect relationship between alpha-synuclein fibrillization and Parkinson's disease? *Nat. Cell Biol.* **2000**, *2* (7), E115−E119.

(9) Harper, J. D.; Wong, S. S.; Lieber, C. M.; Lansbury, P. T. Assembly of A beta amyloid protofibrils: An in vitro model for a possible early event in Alzheimer's disease. *Biochemistry* **1999**, *38* (28), 8972−8980.

(10) Hartley, D. M.; Walsh, D. M.; Ye, C. P. P.; Diehl, T.; Vasquez, S.; Vassilev, P. M.; Teplow, D. B.; Selkoe, D. J. Protofibrillar intermediates of amyloid beta-protein induce acute electrophysiological changes and progressive neurotoxicity in cortical neurons. *J. Neurosci.* **1999**, *19* (20), 8876−8884.

(11) Lambert, M. P.; Barlow, A. K.; Chromy, B. A.; Edwards, C.; Freed, R.; Liosatos, M.; Morgan, T. E.; Rozovsky, I.; Trommer, B.; Viola, K. L.; Wals, P.; Zhang, C.; Finch, C. E.; Krafft, G. A.; Klein, W. L. Diffusible, nonfibrillar ligands derived from A beta(1−42) are potent central nervous system neurotoxins. *P. Natl. Acad. Sci. USA* **1998**, *95* (11), 6448−6453.

(12) Lee, L. Y. L.; Chen, R. P. Y. Quantifying the sequence-dependent species barrier between hamster and mouse prions. *J. Am. Chem. Soc.* **2007**, *129* (6), 1644−1652.

(13) Sampaoli, S.; Agosti, A.; Pozzi, G.; Ciarletta, P. A toy model of misfolded protein aggregation and neural damage propagation in neurodegenerative diseases. *Int. J. Nonlin. Mech.* **2022**, 144.

(14) Walker, L. C.; Jucker, M. Neurodegenerative Diseases: Expanding the Prion Concept. *Annu. Rev. Neurosci.* **2015**, *38*, 87−103.
(15) Dee, D. R.; Woodside, M. T. Comparing the energy landscapes for native folding and aggregation of PrP. *Prion* **2016**, *10* (3), 207−220.
(16) Morriss-Andrews, A.; Shea, J. E. Kinetic pathways to peptide aggregation on surfaces: The effects of beta-sheet propensity and surface attraction. *J. Chem. Phys.* **2012**, *136* (6), 065103.
(17) Yu, H.; Gupta, A. N.; Liu, X.; Neupane, K.; Brigley, A. M.; Sosova, I.; Woodside, M. T. Energy landscape analysis of native folding of the prion protein yields the diffusion constant, transition path time, and rates. *P. Natl. Acad. Sci. USA* **2012**, *109* (36), 14452−14457.
(18) Goldsbury, C.; Kistler, J.; Aebi, U.; Arvinte, T.; Cooper, G. J. S. Watching amyloid fibrils grow by time-lapse atomic force microscopy. *J. Mol. Biol.* **1999**, *285* (1), 33−39.
(19) Hoyer, W. G.; Cherny, D.; Subramaniam, V.; Jovin, T. M. Rapid self-assembly of alpha-synuclein observed by in situ atomic force microscopy. *J. Mol. Biol.* **2004**, *340* (1), 127−139.
(20) Lou, Z.; Wang, B.; Guo, C.; Wang, K.; Zhang, H.; Xu, B. Molecular-level insights of early-stage prion protein aggregation on mica and gold surface determined by AFM imaging and molecular simulation. *Colloids Surf.B: Biointerfaces* **2015**, *135*, 371−378.
(21) Pan, Y.; Wang, B.; Zhang, T.; Zhang, Y.; Wang, H.; Xu, B. Nanoscale insights into full-length prion protein aggregation on model lipid membranes. *Chem. Commun.* **2016**, *52* (55), 8533−8536.
(22) Wang, B.; Guo, C.; Lou, Z.; Xu, B. Following the aggregation of human prion protein on Au(111) surface in real-time. *Chem. Commun.* **2015**, *51* (11), 2088−2090.
(23) van der Kamp, M. W.; Daggett, V. Influence of pH on the human prion protein: insights into the early steps of misfolding. *Biophys. J.* **2010**, *99* (7), 2289−2298.
(24) Lewis, V.; Hooper, N. M. The role of lipid rafts in prion protein biology. *Front. Biosci.* **2011**, *16*, 151−168.
(25) Yin, S.; Pham, N.; Yu, S.; Li, C.; Wong, P.; Chang, B.; Kang, S.-C.; Biasini, E.; Tien, P.; Harris, D. A.; Sy, M.-S. Human prion proteins with pathogenic mutations share common conformational changes resulting in enhanced binding to glycosaminoglycans. *Proc. Natl. Acad. Sci. U. S. A.* **2007**, *104* (18), 7546−7551.
(26) Chesebro, B. Introduction to the transmissible spongiform encephalopathies or prion diseases. *Br. Med. Bull.* **2003**, *66* (1), 1−20.
(27) Rönnberg, E.; Melo, F. R.; Pejler, G. Mast cell proteoglycans. *J. Histochem. Cytochem.* **2012**, *60* (12), 950−962.
(28) Ban, T.; Hamada, D.; Hasegawa, K.; Naiki, H.; Goto, Y. Direct observation of amyloid fibril growth monitored by thioflavin T fluorescence. *J. Biol. Chem.* **2003**, *278* (19), 16462−16465.
(29) Baskakov, I. V.; Legname, G.; Baldwin, M. A.; Prusiner, S. B.; Cohen, F. E. Pathway complexity of prion protein assembly into amyloid. *J. Biol. Chem.* **2002**, *277* (24), 21140−21148.
(30) Vieira, T. C.; Reynaldo, D. P.; Gomes, M. P.; Almeida, M. S.; Cordeiro, Y.; Silva, J. L. Heparin binding by murine recombinant prion protein leads to transient aggregation and formation of RNA-resistant species. *J. Am. Chem. Soc.* **2011**, *133* (2), 334−344.
(31) Ermonval, M.; Mouillet-Richard, S.; Codogno, P.; Kellermann, O.; Botti, J. Evolving views in prion glycosylation: functional and pathological implications. *Biochimie* **2003**, *85* (1−2), 33−45.
(32) Vieira, T. C.; Cordeiro, Y.; Caughey, B.; Silva, J. L. Heparin binding confers prion stability and impairs its aggregation. *FASEB J.* **2014**, *28* (6), 2667−2676.
(33) Huang, P.; Lian, F.; Wen, Y.; Guo, C.; Lin, D. Prion protein oligomer and its neurotoxicity. *Acta biochim. biophys. Sin.* **2013**, *45* (6), 442−451.
(34) Sasaki, K.; Gaikwad, J.; Hashiguchi, S.; Kubota, T.; Sugimura, K.; Kremer, W.; Kalbitzer, H. R.; Akasaka, K. Reversible monomer-oligomer transition in human prion protein. *Prion* **2008**, *2* (3), 118−122.
(35) Silveira, J. R.; Raymond, G. J.; Hughson, A. G.; Race, R. E.; Sim, V. L.; Hayes, S. F.; Caughey, B. The most infectious prion protein particles. *Nature* **2005**, *437* (7056), 257−261.
(36) Tielens, F.; Santos, E. AuS and SH Bond Formation/Breaking during the Formation of Alkanethiol SAMs on Au(111): A Theoretical Study. *J. Phys. Chem. C* **2010**, *114* (20), 9444−9452.
(37) Guo, C.; Wang, B.; Wang, L.; Xu, B. Structural basis of single molecular heparin−FX06 interaction revealed by SPM measurements and molecular simulations. *Chem. Commun.* **2012**, *48* (100), 12222−12224.
(38) Khan, S.; Gor, J.; Mulloy, B.; Perkins, S. J.3IRJ. Solution Structure of Heparin dp24. *Protein Data Bank*2009.
(39) Guo, C.; Fan, X.; Qiu, H.; Xiao, W.; Wang, L.; Xu, B. High-resolution probing heparan sulfate−antithrombin interaction on a single endothelial cell surface: single-molecule AFM studies. *Phys. Chem. Chem. Phys.* **2015**, *17* (20), 13301−13306.
(40) Stroh, C.; Wang, H.; Bash, R.; Ashcroft, B.; Nelson, J.; Gruber, H.; Lohr, D.; Lindsay, S. M.; Hinterdorfer, P. Single-molecule recognition imaging-microscopy. *P. Natl. Acad. Sci. USA* **2004**, *101* (34), 12503−12507.
(41) Evans, E. Probing the relation between force - Lifetime - and chemistry in single molecular bonds. *Annu. Rev. Bioph. Biom.* **2001**, *30*, 105−128.
(42) Wang, C. Z.; Jin, Y. Z.; Desai, U. R.; Yadavalli, V. K. Investigation of the heparin-thrombin interaction by dynamic force spectroscopy. *Bba-Gen Subjects* **2015**, *1850* (6), 1099−1106.
(43) Snow, C. D.; Rhee, Y. M.; Pande, V. S. Kinetic definition of protein folding transition state ensembles and reaction coordinates. *Biophys. J.* **2006**, *91* (1), 14−24.
(44) Harris, N. C.; Song, Y.; Kiang, C. H. Experimental free energy surface reconstruction from single-molecule force spectroscopy using Jarzynski's equality. *Phys. Rev. Lett.* **2007**, *99* (6), 068101.
(45) Bilsel, O.; Robert Matthews, C. Barriers in protein folding reactions. *Adv. Protein Chem.* **2000**, *53*, 153−207.
(46) Baskakov, I. V.; Legname, G.; Prusiner, S. B.; Cohen, F. E. Folding of prion protein to its native alpha-helical conformation is under kinetic control. *J. Biol. Chem.* **2001**, *276* (23), 19687−90.

https://doi.org/10.1021/acsabm.2c00779
ACS Appl. Bio Mater. 2022, 5, 5457−5464